Applied Nanoscience
https://doi.org/10.1007/s13204-022-02608-1

ORIGINAL ARTICLE

Estimation of in vivo toxicity of MgO/ZnO core/shell nanoparticles synthesized by eco-friendly non-thermal plasma technology

Raghad S. Mohammed[1] · Kadhim A. Aadim[2] · Khalid A. Ahmed[1]

Received: 4 February 2022 / Accepted: 13 August 2022

Abstract

MgO/ZnO core/shell nanoparticles were synthesized using the atmosphere plasma jets technique. The physical properties of the synthesized nanoparticles were investigated by a series of techniques, including X-ray diffraction (XRD), X-ray dispersive spectroscopy (EDS), and transmission electron microscopy (TEM). XRD and EDS analyses confirmed the purity of the nanoparticles synthesized with an average nanoparticle crystallite size of 36 nm. TEM confirmed the successful synthesis of spindle-shaped MgO/ZnO core/shell nanoparticles with an average size of 70 nm. To evaluate their toxicity, the MgO/ZnO core/shell nanoparticles were tested in vivo. Twenty-five albino female rats were randomly divided into five groups (five rats in each group); one was used as the control group and the other four as the experimental groups. Doses of the MgO/ZnO core/shell nanoparticles solution were orally administered to the test groups to examine the toxicity. For 30 consecutive days, each rat in test groups 2–5 received 1 mL of the MgO/ZnO core/shell nanoparticles solution at the respective doses of 1.25, 2.5, 5, and 10 mg L^{-1}. The rats' growth, hematology, thyroid gland function, and histopathology were examined after 30 days. Findings indicate that the growth retardation in the rats treated with MgO/ZnO core/shell nanoparticles may be due to their infection by *Hyperthyroidism*. The hematology results show the nonsignificant effect of MgO/ZnO core/shell nanoparticles on white blood cells, implying that these nanoparticles have no harmful impact on the immune system. Moreover, the levels of the thyroxine and thyroid-stimulating hormones increased, and that of the triiodothyronine hormone decreased. The histological analysis results show that low concentrations of MgO/ZnO core/shell nanoparticles are safe for desired biomedical applications.

Keywords Non-thermal plasma · In vivo toxicity · Albino rats · Hematology · Histopathology · Thyroid hormones

Abbreviations

NPs	Nanoparticles
MNPs	Metal nanoparticles
NM	Nano metal
CS	Core/shell
Ar	Argon
Wt%	Weight percentage
KV	Kilo Volt
Hz	Hertz
nm	Nanometer
ROS	Reactive oxygen species
RBC	Red blood cells
WBC	White blood cells
HCT	Hematocrit
Hb	Hemoglobin
MCH	Mean corpuscular hemoglobin
MCV	Mean corpuscular volume
MCHC	Mean corpuscular hemoglobin concentration
T3	Triiodothyronine hormone
T4	Thyroxine hormone
TSH	Thyroid stimulating hormone
H	Hematoxylin stain
E	Eosin stain
P value	Significant value
SD	Standard deviation
Mg L^{-1}	Milligram per litter

✉ Raghad S. Mohammed
raghad.almaliki@uomustansiriyah.edu.iq

[1] Department of Physics, College of Science, Mustansiriyah University, Baghdad, Iraq

[2] Department of Physics, College of Science, University of Baghdad, Baghdad, Iraq

Published online: 13 September 2022

Introduction

Nanotechnology is a burgeoning field that enables the creation of novel materials and/or devices in the nanometer size range (1–100 nm) for various applications. This revolutionary technology can improve nearly every aspect of human life, including medical healthcare (Ahamed et al. 2015; Jeyaraj et al. 2019). Nanoparticles (NPs) are in high demand in the global market, and the demand is estimated to exceed 98 billion dollars by 2025. Numerous technologies from various sources, such as physical, chemical, and biological materials, are involved in the fabrication of nanomaterials (Jeyaraj et al. 2019). Plasma synthesis is currently used in various applications (Jang et al. 2021), such as surface modification (Hegemann et al. 2016; Rao et al. 2018), layer deposition for electrical devices (Seo et al. 2019), and anti-bio or bio-material applications (Vasilev 2013; Vasani et al. 2017). Compared to chemical synthesis, the non-thermal plasma synthesis of metal nanostructures is a green synthesis technology with significant advantages. Non-thermal plasma is a beneficial alternative to synthesizing NPs because no toxic agents are used, and the processing time is shorter than that required for chemical synthesis (Chiang et al. 2019; Kaushik et al. 2019). This technology generates large amounts of free electrons, charged particles, excited metastable species, reactive oxygen, and nitrogen species through non-thermal atmospheric pressure plasmas in ambient conditions (Bruggeman et al. 2016). When the plasma comes into contact with the liquid medium, these species can be transported into the liquid phase (Rumbach et al. 2013, 2015). The chemical reactions during the plasma synthesis of metallic NPs (MNPs) in plasma-activated water depend primarily on the dissolved reactive species (Chen et al. 2015; Rumbach and Go 2017). MNPs mainly include metal and metal oxide NPs. Given their unique features, MNPs have attracted considerable commercial attention with the development of nanotechnology. Thus, their potential toxic effects on human health and the environment have received significant attention (Sajid et al. 2014; Yao et al. 2019).

Silicon dioxide (SiO_2), titanium dioxide (TiO_2), ferric oxide ($Fe2O_3$), magnesium oxide (MgO), and zinc oxide (ZnO) are the most important representatives of the single metal oxide group. Because of their unique features, these materials have uses in fields such as electronics, information technology, energy, agriculture, medical, and environmental protection (Hornak 2021). Among the metal oxide nanoparticles, magnesium oxide (MgO) is of great interest for many reasons, including the fact that they are abundant, stable, inexpensive, odorless, and non-toxic (Chinthala et al. 2021). Additionally, ZnO was used in ointments to treat adverse skin conditions since at least 2000 B.C., in ancient Egypt and then in Rome (Borysiewicz 2019). ZnO NMs have many potential medical applications, including contrast agents (imaging), diagnostic and therapeutic functions, in photodynamic therapy, biosensor, prophylactic and therapeutic vaccines, gene carriers, drug carriers, iron delivery, potential anti-cancer agent, wound dressing, tissue engineering, support for antifungal treatments, and inhibition of influenza virus infection (Wojnarowicz et al. 2020).

According to previous studies, the systemic administration of diagnostic or therapeutic metal oxide NPs often results in significant bioaccumulation in the liver and the possibility of NPs interactions with hepatic cells. Thus, safety screening methodologies should be developed for the interactions of metal oxide NPs with the liver and other organs (Mirshafiee et al. 2018). During the past decade, many studies have been reported on coating NPs with different organic and inorganic agents, such as polymers, organic monolayers, oxides, and metals, to create core/shell (CS) MNPs. CS NPs have recently gained increasing attention due to their low cytotoxicity and chemical liable surface (Sabale et al. 2017; Rajabi and Sohrabnezhad 2018). These studies focused on inorganic shells, like noble metals, carbon, and silica and demonstrated many biomedical applications (Sabale et al. 2017). Some of these studies investigated the plasma synthesis of hybrid nanomaterials composed of Au NPs and a polymer to improve the stability and biocompatibility of Au NPs (Nguyen et al. 2020; Jang et al. 2021). Metal nanomaterials are an important gateway to medicine's future. MgO and ZnO NPs within various biomedical applications have already found their place. Thus, in this study were selected these nanomaterials to create core/shell NPs to modify and cause changes in their characteristics and reduce toxicity. Studies have also reported the toxicity of MgO (Mangalampalli et al. 2017; Mangalampalli et al. 2018) and ZnO NPs (Almansour et al. 2017; Singh et al. 2019). To the best of our knowledge and according to a literature survey, no report is available on the acute lethal effect and toxicity of biologic MgO/ZnO CS NPs. However, the toxicity of MgO/ZnO CS NPs must be carefully researched, and their toxicity mechanisms must be clarified before their commercial implementation in biomedical applications. Thus, the present study's biomedical application includes the estimation of toxicity via hematology, thyroid hormones, and histopathology analyses.

Methods

Synthesis nanoparticles

To synthesize MgO/ZnO CS NPs, we used a magnesium wire and a zinc sheet with a purity content of 99.99%, purchased from (THE BRITISH DRUG HOUSES LTD./

LONDON, Manufactured in England, 652247/470611). As shown in Fig. 1, the experimental setup consists of a high voltage DC power supply (20 kV) and a stainless steel tube that acted as the cathode. A magnesium wire or zinc sheet was used as the anode, immersed in a glass beaker containing 5 mL of deionized water. The Ar gas flow was fixed at 2 L min^{-1} using a flowmeter; the plasma jet propagated across the air at a distance of approximately 2 cm between the plasma jet nozzle and the surface of deionized water. The plasma treatment of the metal in the liquid lasted for 5 min. MgO/ZnO CS NPs were synthesized in two steps. First, magnesium was used as the electrode to synthesize the MgO cores. Second, the ZnO shell around the MgO cores was synthesized by replacing the magnesium with a zinc electrode. The synthesized MgO/ZnO CS NPs were characterized by techniques, including XRD (XPERT PAANALTICAL PHILLIPS HOLLAND), EDS (TESCN MIRA3 FRENCH), and TEM, which were carried out in Iran at the University of Kashan.

Animals and condition

Healthy 5-week-old albino female rats weighing 65–90 g were purchased from the *University of Al-Nahrain/Biotechnology Research Center/Animal House*. The rats were housed in plastic cages in an air-conditioned room at 12-h light and 12-h dark cycle. The room's temperature ranged from 22 to 24 °C ± 2 °C. The rats had free access to food and water. Twenty-five rats were randomly divided into five groups (five rats in each group), with one group assigned as the control group and the remaining four as test groups, and administered various doses of MgO/ZnO CS NPs. After a 1-week acclimatization period, the animals were 6 weeks old at the start of the experiment. The control group female rats were not treated. Different doses of the MgO/ZnO CS NPs solution were orally administered to the test groups to examine the toxicity. Every day, each rat in test groups 2–5 received 1 mL of the MgO/ZnO CS NPs solution at 10, 5, 2.5, and 1.25 mg L^{-1} doses. Each rat was observed twice daily for any clinical signs of toxicity, and the body weight was measured each week throughout the test period. The rats were sacrificed after 30 days to examine the toxicity through hematological, thyroid hormones, and histological analyses.

Haematological analysis

Blood samples were collected through an intra-cardiac puncture after the inhalation of anesthesia with *isoflurane* (*manufactured by Piramal Enterprises Limited: Telangana, India*). The blood samples were immediately collected in coated tubes for hematological analysis. The hematological parameters were examined: red blood cells (RBCs), white blood cells (WBCs), hematocrit (HCT), hemoglobin (Hb) levels, mean corpuscular hemoglobin (MCH), mean corpuscular volume (MCV), and mean corpuscular hemoglobin concentration (MCHC).

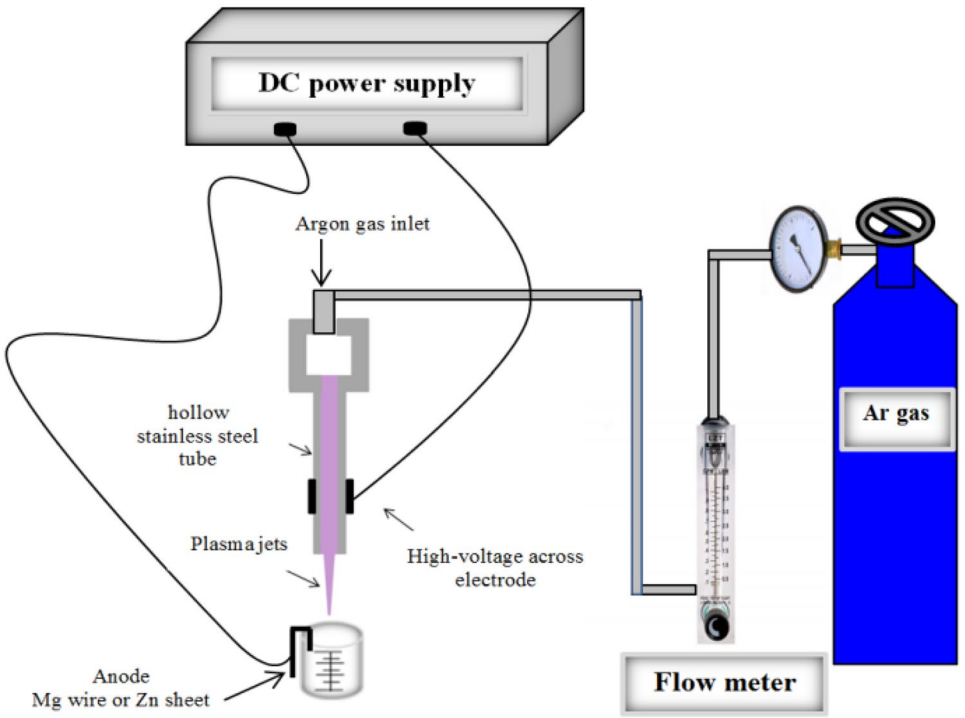

Fig. 1 The experimental setup of a non-thermal plasma system to synthesize MgO/ZnO CS NPs

Thyroid hormones analysis

Blood samples were collected in clotted vials to estimate the serum biochemical examination. The serum was collected by centrifugation for 10 min at 2000 rpm in an automatic analyzer (Hitachi 912 Chemistry Analyzer). The thyroid gland activity was assessed through the triiodothyronine (T3), thyroxin (T4), and thyroid-stimulating hormone (TSH) levels using the serum.

Histopathology analysis

Histological analysis was performed to determine whether the MgO/ZnO CS NPs caused morphological changes in the kidney, liver, and spleen of the rats. Tissue specimens were collected and washed with deionized water to remove the blood and then fixed in 10% formalin, embedded in paraffin blocks, and cut into sections of 5 µm thickness. Hematoxylin and eosin (H and E) staining was performed to analyze the fixed sections. The sections were examined under a binocular microscope (40, 100, and 400× magnification), and photomicrographs of the fixed tissue were taken.

Statistical analysis

The results of each group are expressed in mean ± standard deviation ($n = 5$), and all the experimental values were compared with the corresponding control values. The results presented as mean ± standard deviation by ANOVA followed by GraphPad Prism version 8 (GraphPad Software Inc., La Jolla, CA, USA) were used to analyze the differences between the mean values and P value ≤ 0.05 was considered statistically significant.

Result and disscusion

Characterization of MgO/ZnO core/shell nanoparticles

The XRD pattern of the MgO/ZnO CS NPs was recorded at a 2θ° angle ranging from 30° to 60°, as shown in Fig. 2a. The broad diffraction peaks appear at angles positions 31.40°, 34.1, 36.3, 47.7, and 56.94, which are related to the ZnO structure and are indexed to miller indices (100), (002), (101), (102),

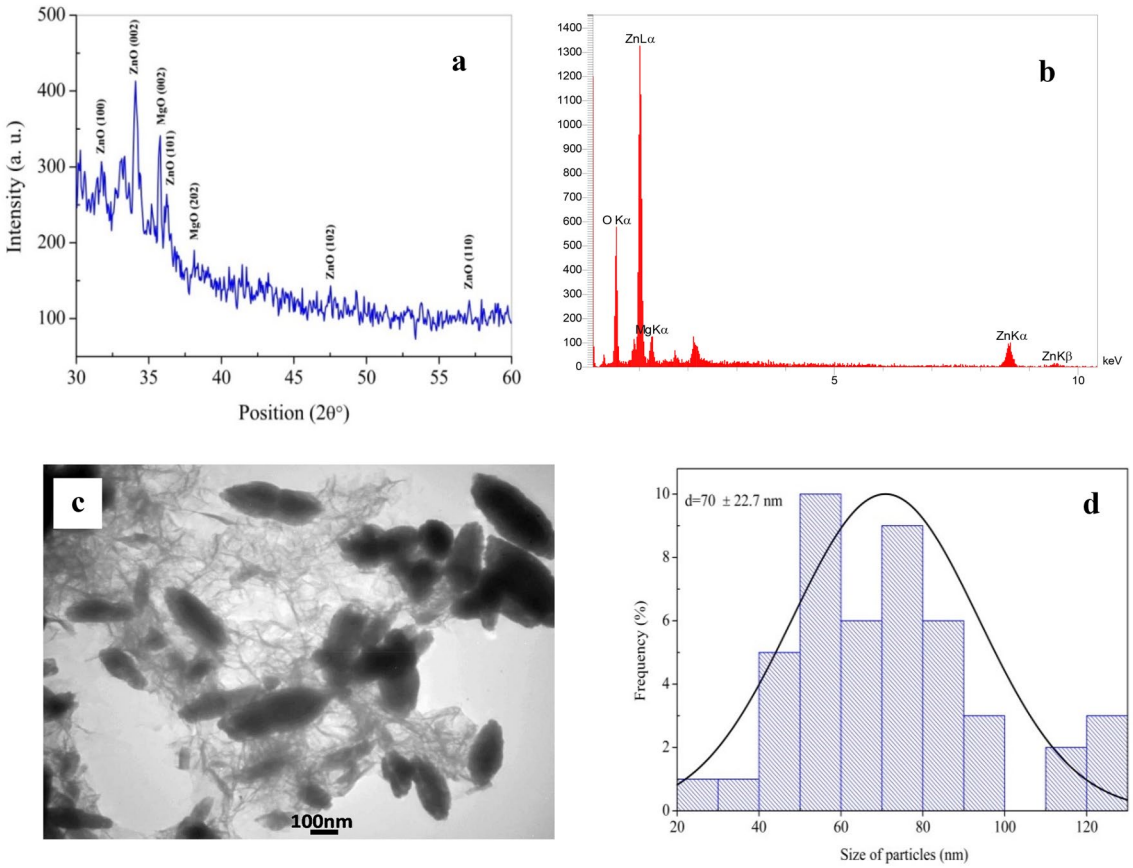

Fig. 2 Physical properties of MgO/ZnO CS NPs synthesized with non-thermal plasma jet. **a** XRD pattern, **b** EDS pattern, **c** TEM image, **d** size of particles histogram

and (110), respectively. Have been matched with the JCPDS No: 36-1451 of the zinc oxide hexagonal wurtzite structure. While, diffraction peaks at 2θ° positions 36.1° and 38.13° are found to be relative to (002) and (202) planes, respectively, of MgO, were matched with the JCPDS No: 87-0653, which appear the creation of MgO polycrystalline cubic structure. The XRD pattern of MgO/ZnO did not appear any other peaks related to secondary phases for MgO and ZnO that indicate the purity of the synthesized sample. The crystalline size of MgO/ZnO CS NPs was measured from the Scherrer equation (Ali et al. 2017)

$$D(^{\circ}A) = \frac{k\lambda}{\beta\cos\theta}$$

Here D is the average crystalline size, k is the Scherer's constant ($k=0.9$), λ is the X-rays wavelength (1.540 Å), and β is the full width at half maximum (FWHM) of the peaks at diffracting angle θ from the Bragg's angle position. The average crystalline size of MgO/ZnO CS NPs is 36 nm.

EDS analyses

The chemical composition of the synthesized MgO/ZnO CS NPs was examined using Energy Dispersive X-Ray Spectroscopy (EDS). Figure 2b show the EDS spectrum analysis revealed the presence of Zn, Mg, and O, indicating that the sample formed was pure successfully, with no impurity elements present in MgO/ZnO CS NPs. The percentages of compositions (weight%) of the Mg, Zn, and O were 5.33%, 57.27%, and 37.40%, respectively. Also, the percentages of compositions (atomic %) were 6.38, 25.52, and 68.0 for Mg, Zn, and O, respectively.

TEM analysis

Transmission Electron Microscopy (TEM) analysis has been carried out to confirm the synthesis of the core/shell nanoparticles. The information relevant to the shape, size, and aggregation was obtained from TEM analysis. The TEM images show that the MgO/ZnO CS NPs are spindle-shaped, as shown in Fig. 2c. In addition, it demonstrated that there are two different regions inner dark part represents the core. The shiny part surrounding the dark region represents the shell, confirming the synthesis of MgO/ZnO CS NPs. The Image J software program carried out the analysis of the TEM image to determine the particle size. The average diameter of MgO/ZnO CS NPs is 70 nm, as shown in the size distribution histogram Fig. 2d.

Assessment toxicity

In vitro cultures seem unable to include helpful information about the physiological system response under investigation. Thus, examining the in vivo toxicity is beneficial for synthesizing MgO/ZnO CS NPs through the plasma jets technique.

Animal observation

Each animal was observed twice daily for any clinical signs of toxicity or mortality throughout the test period. During the treatment period, no mortality was observed. Except for growth retardation, pupil changes, and hair loss in some groups, the animals in all the groups did not show severe clinical poisoning symptoms, like loss of appetite, skin color change, and decreased mobility. The rats were weighed every week during the experiment. Figure 3 shows the mean body weights ± SD of the groups treated with MgO/ZnO CS NPs at various doses compared with the control group. The outcomes indicate the growth retardation of the female rats, which can be attributed to the rats' injury from *Hyperthyroidism,* as discussed in the section on thyroid hormones. Growth retardation is the main characteristic of NP-intoxicated animals. The American National Research Council reported that growth inhibition might be the greatest sign of NPs' toxicity. NPs reduce the production of growth hormone, somatomedin C, insulin-like growth factor-binding proteins, and insulin-like growth factor-I, causing growth retardation (Shakibaie et al. 2013).

Hematology analysis

The assessment of hematological parameters is an essential step in the detection of the toxicity of NPs. After 30 days of oral exposure to MgO/ZnO CS NPs at various concentrations, the hematological profiles were assessed to determine the physiological state of the animals. Hematological parameters can be used to diagnose the extent of a foreign compound's harmful influence on an animal's blood constituents. Given that changes in the hematological system have a high predictive value for toxicity, such toxicity testing is relevant

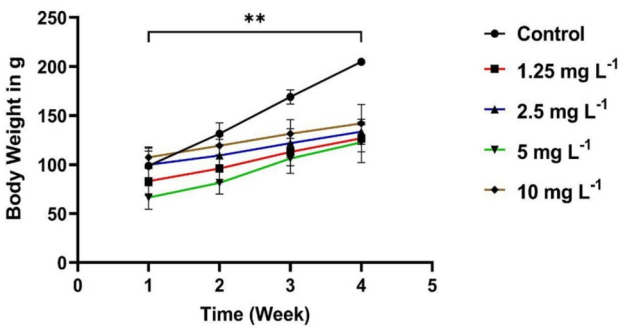

Fig. 3 Mean body weight of female rats administered MgO/ZnO CS NPs at the doses of 1.25, 2.5, 5, and 10 mg L^{-1} for 30 consecutive days. Values are means ± SD ($n=5$), (** refer $P<0.01$, compared with the control)

to risk assessment when data from animal studies are translated into human toxicity (Ashafa et al. 2012).

Table 1 shows the concentration-dependent hematology results of the MgO/ZnO CS NPs. The hematologic parameters reveal that the Hb levels were affected only at the 1.25 mg L^{-1} dose and the HCT at the 2.5, 5, and 10 mg L^{-1} doses. In contrast, the MCHC was affected at all doses. The disturbing normal cell physiology shows abnormal oxygenation from the lungs, indicating the absence of oxygen in the blood with elevated Hb and HCT values (Espinosa-Cristobal et al. 2013; Mangalampalli et al. 2018). Although these values are regarded as normal parameters, further studies should focus on them. No effect was observed on the other hematologic parameters compared with the control groups. The non-significant impact of MgO/ZnO CS NPs on WBCs implies that the rates of hematological parameter entry into the blood from the bone marrow and removal from circulation were unchanged (Aluko et al. 2017). This practical implication indicates that the MgO/ZnO CS NPs NPs have no harmful impact on the immune system. Figure 4 presents the mean value of the hematologic parameters ± SD of the groups treated with MgO/ZnO CS NPs at various doses compared with the control group. Changes in blood cells occur when blood component anomalies interfere with normal functions (Khabbazi et al. 2015).

Thyroid hormones function

The toxic effect of MgO/ZnO CS NPs on thyroid gland function, the concentrations of thyroid hormones (T3 and T4), and the TSH were analyzed in the blood serum of albino female rats in control and treated groups after 30 days. The analysis revealed that the T3 level decreased while the T4 and TSH levels increased, as reported in Table 2. Although MgO/ZnO CS NP exposure affected the serum T3 concentrations, statistically significant differences in the T4 levels were found only in the group treated with the 1.25 mg L^{-1} dose ($P < 0.0137$). The T3 levels decreased when the exposure dosage increased. The statistically significant differences in T3, T4, and TSH in the serum blood due to the oral administration of MgO/ZnO CS NPs are shown in Fig. 4. However, these results have highlighted a significant practical implication, the increase in the T4 level indicates that the rats were infected by *Hyperthyroidism*, which explains their weight reduction. Hyperthyroidism is a catabolic state related to increased energy consumption, protein turnover, and lipolysis. Usually, these metabolic effects result in weight reduction, accompanied by a decrease in fat storage and lean body mass (Peterson et al. 2016). The results of our study are partly consistent with those of a recent survey reported by (Sakr and Steenkamp 2021), who found a significant reduction in triiodothyronine (T3), thyroxine (T4), and TSH after 30 days of exposure to zinc oxide NPs (200 mg kg^{-1}). The present study demonstrated that exposure to MgO/ZnO CS NPs deteriorates thyroid hormones (T4, T3, and TSH). This finding can be related to increased free radical levels and decreased antioxidants (Yousef et al. 2019). The statistically significant differences in T3, T4, and TSH in serum blood due to the oral administration of the MgO/ZnO CS NPs are shown in Fig. 5.

Histopathological analysis

To assess the toxicity of MgO/ZnO CS NPs, histological analysis was performed on the liver, kidney, and spleen of the female rats after 30 days of consecutive oral administration. The liver and kidney are common target organs regardless of exposure routes and animal types. The results of the histological analysis of these organs are presented below.

Hepatic toxicity

The histological photographs related to the liver of albino female rats in the control group show that the central vein and hepatic cords were normally arranged; the hepatic lobules, the hepatocytes, the sinusoids, and the Kupffer cells were also normal, as shown in Fig. 6a. In the rats treated with MgO/ZnO CS NPs at a dose of 1.25 mg L^{-1}, the sections of hepatic lobules showed regularly arranged hepatic cords and central vein compared with sections of the control group. The magnified sections reveal mild dilation and congestion of the sinusoid and mild sinusoidal infiltration of mononuclear leukocytes, as shown in Fig. 6b. In addition, at the 2.5 mg L^{-1} dose, the magnified sections

Table 1 Hematological parameters in female rats treated with various doses of MgO/ZnO core/shell NPs

Hematological parameters	Control Mean ± SD	1.25 (mg L^{-1}) Mean ± SD	2.5 (mg L^{-1}) Mean ± SD	5 (mg L^{-1}) Mean ± SD	10 (mg L^{-1}) Mean ± SD
WBC	17.00 ± 0.685	12.95 ± 5.297	12.63 ± 3.754	11.86 ± 6.337	11.52 ± 2.750
RBC	5.386 ± 0.326	5.254 ± 0.584	5.668 ± 0.451	5.138 ± 0.472	5.944 ± 0.943
Hb	10.40 ± 0.158	14.06 ± 3.343	12.82 ± 1.045	11.24 ± 1.026	13.06 ± 2.053
MCV	41.06 ± 19.94	54.14 ± 5.663	54.22 ± 1.089	54.22 ± 4.130	54.72 ± 1.574
MCH	20.24 ± 0.623	23.34 ± 0.760	22.56 ± 0.907	21.86 ± 1.346	21.90 ± 0.640
MCHC	41.86 ± 0.397	41.74 ± 1.036	41.76 ± 1.266	40.42 ± 1.571	40.16 ± 1.328

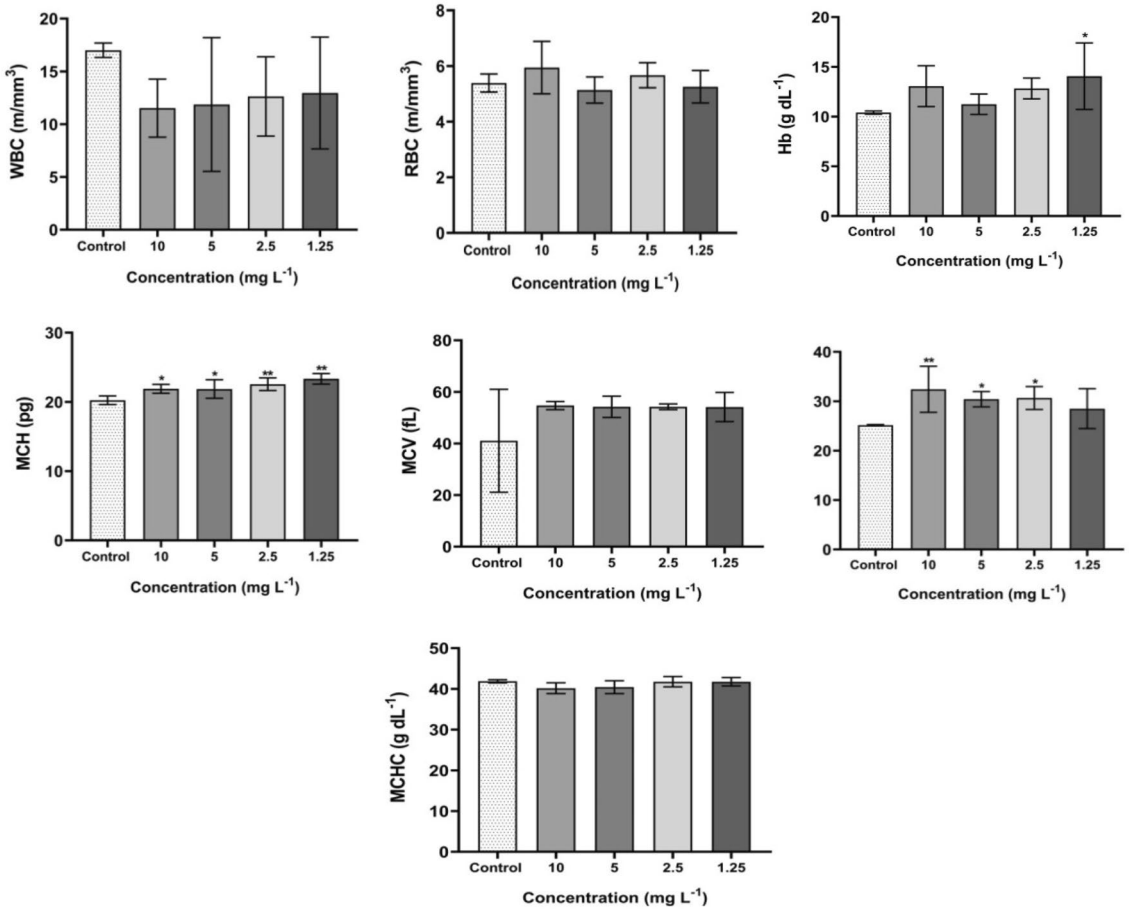

Fig. 4 The hematological results for rats treated with MgO/ZnO core/shell nanoparticles following 30 days at different doses (1.25, 2.5, 5, and 10 mg. L^{-1}). Values are means ± SD ($n = 5$) (* refer $P < 0.05$ and ** refer $P < 0.01$, compared with the control group)

Table 2 Results of effect thyroid hormones in female rats exposed to various doses of MgO/ZnO CS NPs

Thyroid hormones	Control Mean ± SD	1.25 (mg L^{-1}) Mean ± SD	2.5 (mg L^{-1}) Mean ± SD	5 (mg L^{-1}) Mean ± SD	10 (mg L^{-1}) Mean ± SD
T3	2.568 ± 0.256	2.576 ± 0.188	2.546 ± 0.146	2.104 ± 0.241	1.976 ± 0.196
T4	41.96 ± 8.200	59.29 ± 9.495	50.83 ± 5.270	46.71 ± 8.354	46.85 ± 9.974
TSH	0.2442 ± 0.1189	0.081 ± 0.018	0.095 ± 0.014	0.097 ± 0.015	0.134 ± 0.048

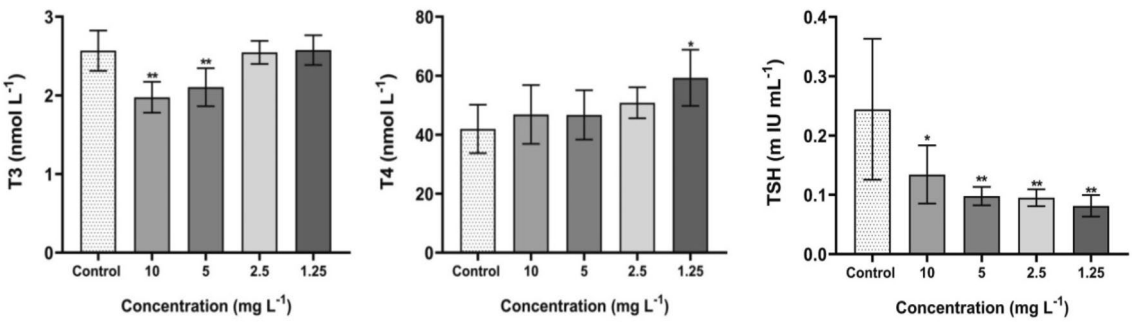

Fig. 5 Thyroid hormones (T3, T4, TSH) for rats treated with MgO/ZnO CS NPs following 30 days at different doses (1.25, 2.5, 5, and 10 mg L^{-1}). Values are means ± SD ($n = 5$) (* refer $P < 0.05$ and ** refer $P < 0.01$, compared with the control group

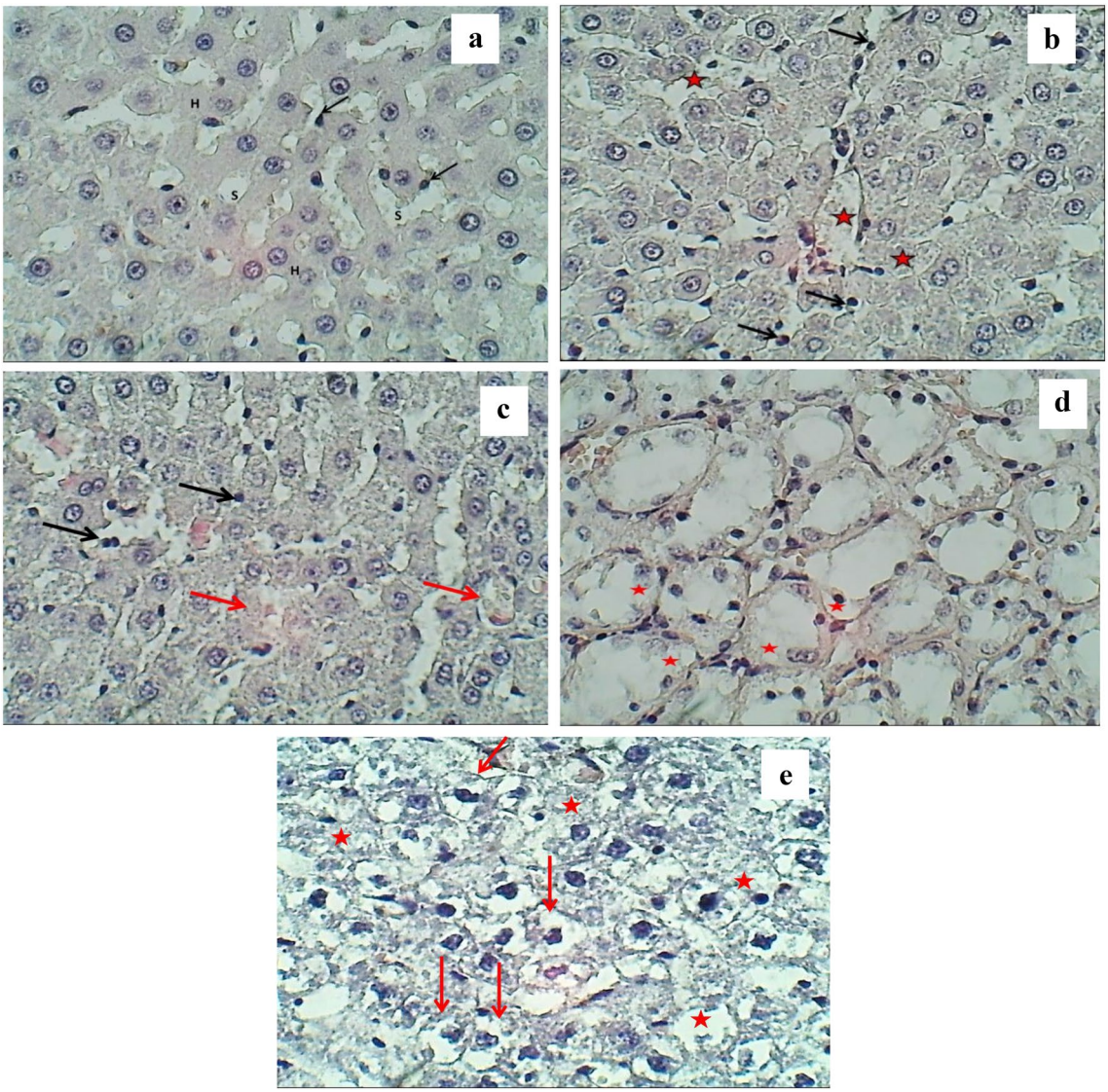

Fig. 6 Histological results of the liver (H and E stained, ×400 magnification). **a** No abnormal histological changes were observed for hepatocytes (H), sinusoids (S), and kupffer cells (Arrow) in the control group, **b** histological results of the liver after 30 days of oral exposure to MgO/ZnO CS NPs with 1.25 (mg L^{-1}) doses, sections were shows mild infiltration of mononuclear leukocytes (Arrows) and mild dilation with congestion of sinusoids (asterisks), **c** at 2.5 (mg L^{-1}) doses, sections were showed mild infiltration of mononuclear leukocytes (black arrows) and congestion of sinusoids (red arrows), **d** at 5 (mg L^{-1}) doses sections were showed moderate cellular swelling with granular degeneration (asterisks) and necrosis (N) of hepatocytes, **e** at 10 (mg L^{-1}) doses the sections of hepatic lobule show moderate cellular swelling (arrows) and necrosis of hepatocytes (asterisks)

reveal normal hepatocytes, mild dilation and congestion of the sinusoid, and mild sinusoidal infiltration of mononuclear leukocyte as shown in Fig. 6c. The histopathological analysis indicates that exposure to 5 and 10 mg L^{-1} doses induced changes in the liver tissue. The sections of hepatic lobules at the 5 mg L^{-1} dose showed irregularly arranged hepatic cords and moderate cellular swelling with granular cytoplasmic degeneration of hepatocytes, as shown in Fig. 6d. The magnified sections of hepatic lobules at the 10 mg L^{-1} dose reveal irregular arranged hepatic cords, moderate zonal cellular swelling, and the necrosis of hepatocytes, as shown in Fig. 6e. MNPs cause cell damage and death via hepatocyte necrosis by generating reactive oxygen species (ROS). The necrosis of parenchymal cells in organs is promoted by inflammation. Thus, one of the prominent features of acute liver injury is necrosis. Plasma membrane rupture, mitochondrial swelling, and intracellular contents release are all characteristics of necrosis (Yao et al. 2019). The results of the histological analysis indicate that hepatocytes necrosis was induced at 5 and 10 mg L^{-1} of MgO/ZnO CS NPs.

Renal toxicity

The renal sections of the female rats in the control group were normal, as shown in Fig. 7a. Compared to the renal sections of the control group, the renal sections of the rats were administered with 1.25 mg L^{-1} of MgO/ZnO CS NPs revealed no histological changes. The cortex and medulla of the treated rats were similar to those in the control group, as shown in Fig. 7b. In the rats treated with a 2.5 mg L^{-1} dose, the renal cortex sections showed a mild cloudy degeneration of renal tubules. In contrast, the renal medulla showed mild vascular degeneration and necrosis, as shown in Fig. 7c. The renal glomeruli appeared normal in the rats treated with a 5 mg L^{-1} dose. However, the renal cortex and medulla sections showed a mild vascular degeneration of renal tubules, as shown in Fig. 7d. No histological alterations

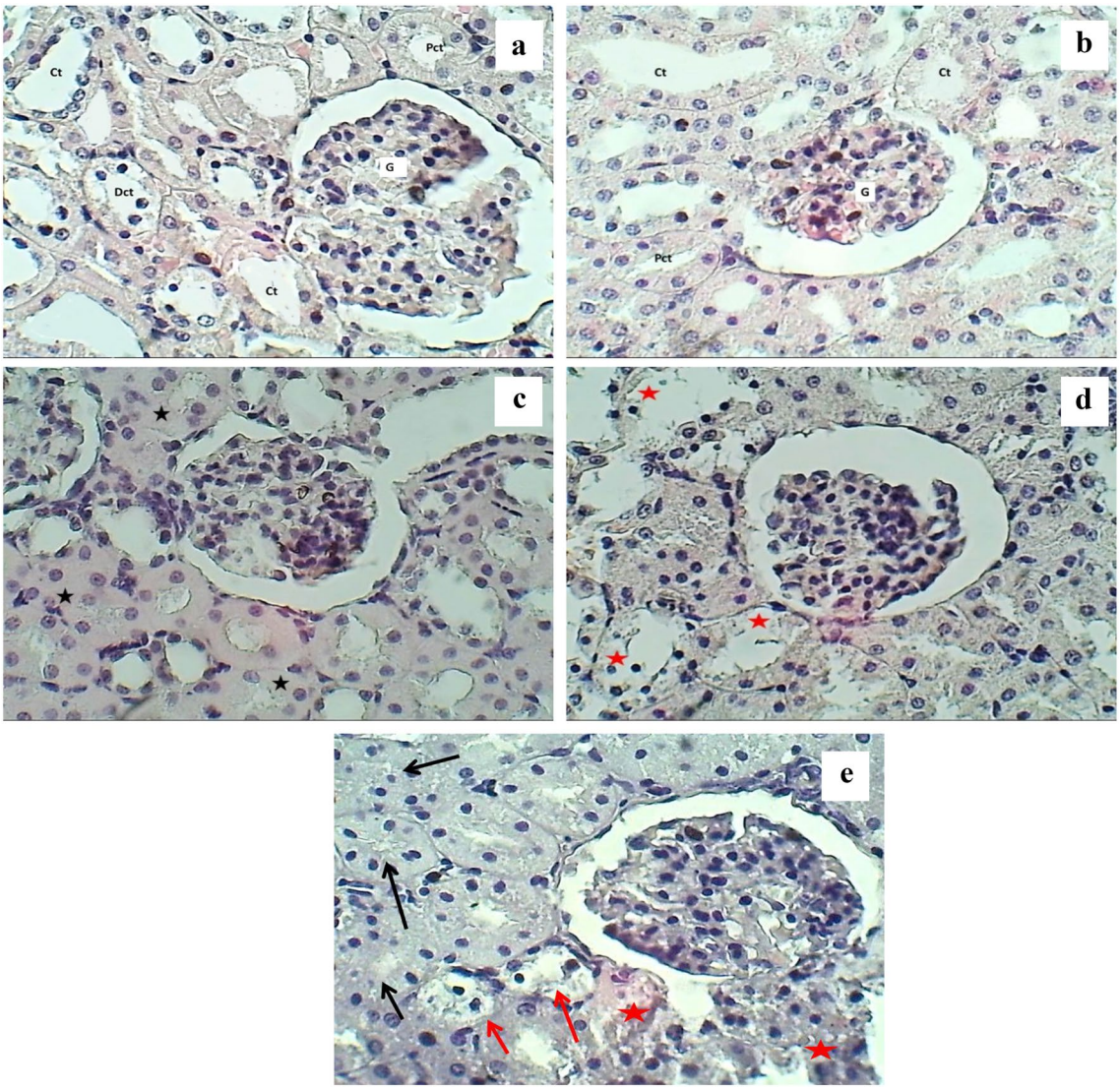

Fig. 7 Histological results of the kidney (H and E stained, ×400 magnification), **a** Section of the renal cortex shows glomeruli (G), collecting tubule (Ct), proximal (Pct), and distal convoluted tubules (Dct) were normal, no abnormal histological changes were observed for hepatocytes (H), sinusoids (S), and kupffer cells (Arrow), **b** histological results of the kidney after 30 days of oral exposure to MgO /ZnO CS NPs with 1.25 (mg L^{-1}) doses, Section of the renal cortex shows collecting tubules, thick segment and thin segment of the Henle loop were normal, no changes of a section of the renal cortex, show glomeruli (G), collecting tubule (Ct), proximal (Pct), and distal convoluted tubules (Dct) were normal, **c** at 2.5 (mg L^{-1}) doses. section of the renal cortex shows mild cloudy degeneration of renal tubules (asterisks) and necrosis (N), section of renal medulla shows mild vacular degeneration of renal tubules (asterisks) and necrosis (N), **d** at 5 (mg L^{-1}) doses section of renal medulla shows mild vacular degeneration of renal tubules (asterisks) and necrosis (N), and Section of renal cortex shows mild vacular degeneration of renal tubules (asterisks), **e** at 10 (mg L^{-1}) doses the Section of the renal cortex shows cloudy degeneration (red arrow) and vacular degeneration (black arrows). Section of renal cortex shows cloudy degeneration (black arrow), vacular degeneration (red arrows) and necrosis of renal tubules (asterisks)

were observed in the renal glomeruli of the rats exposed to a 10 mg L^{-1} dose. However, the renal cortex and medulla sections showed a mild cloudy and vascular degeneration with the renal cortex and little medulla necrosis of the renal tubules, as shown in Fig. 7e.

Splenic toxicity

The splenic sections of the rats in the control group were normal, as shown in Fig. 8a. In comparison to sections of the control group Fig. 8a, the tissue of rat's splenic treated with 1.25 mg L^{-1} of MgO/ZnO CS NPs appears some histological changes. The white pulp of the spleen showed marked enlarged lymphatic follicles associated with the marked hyperplasia of lymphocytes within the germinal center, revealing many mitotic figures. On one hand, the splenic sinusoids within the red pulp revealed severe dilation and congestion, as demonstrated in Fig. 8b. The rats treated with a 2.5 mg L^{-1} dose revealed histological changes in the spleen. The sections of white pulp showed marked enlargement and fused lymphatic follicles associated with the marked hyperplasia of lymphocytes.

On the other hand, the splenic sinusoids within the red pulp revealed severe dilation, congestion, and the marked grouping of non-malignant hyperplastic lymphocytosis, as shown in Fig. 8c. Figure 8d shows the spleen change in the female rats treated with a 5 mg L^{-1} dose. The sections of the splenic white pulp showed marked enlargement and fused lymphatic follicles associated with the marked hyperplasia of lymphocytes. Meanwhile, the female rats treated with a 10 mg L^{-1} dose showed splenic sections with normal splenic white and red pulps, as shown in Fig. 8e.

In terms of toxicity, the results obtained indicate that MgO/ZnO CS NPs are less toxic than previously reported in the literature. Almansour (Almansour et al. 2017) reported that the exposure of male rats to ZnO NPs (35 nm) for 21 days caused the dysfunction liver and kidney tissues and ZnO NPs induced inflammatory cell infiltration, sinusoidal dilatation, Kupffer cells hyperplasia, necrosis, hepatocytes hydropic degeneration, nuclear alterations, and hepatocytes glycogen depletion. Singh (Singh et al. 2019) also reported the oral exposure of rats to a high dose (250 mg kg^{-1}) of ZnO NPs (30 nm) for 28 days might cause the apoptotic death of their splenocytes, indicating that ZnO NPs induced tissue damage via oxidative stress by increasing the generation of ROS, thereby compromising the integrity of cellular membranes.

In addition, few follow-up studies on MgO NPs have demonstrated liver and renal tissue changes in female rats post-acute oral exposures, according to (Mangalampalli et al. 2017); the administration of 2000 mg kg^{-1} of MgO NPs (52.97 nm) for 14 days induced hepatic degeneration and necrosis, and the kidneys revealed focal tubular damage and swelling in the renal glomerulus. The spleen, the heart, and the brain were not affected morphologically. Mangalampalli (Mangalampalli et al. 2018) also found that the oral administration of MgO NPs in 59.85 nm size for 28 days at various doses (250, 500, and 1000 mg kg^{-1}) altered the biochemical and genotoxic parameters of the rats. The liver, kidney, and stomach tissues of the rats that received 1000 mg kg^{-1} of MgO NPs showed severe histopathological damage. The practical implication of the histopathology mentioned findings showed that MgO/ZnO CS NPs could induce morphological and histological changes in the liver, kidneys, and spleen. The damage of this change is much lower and milder than that reported in the literature related to the toxicity of MgO and ZnO. This discrepancy might be due to various factors, like the size of particles and the doses. This finding also suggests that covering MgO NPs with ZnO NPs improves their toxicity properties.

Limitations of the study

The results of this study have to be seen in the light of several potential limitations:

1. The first limitation concerns the conditions of the study conducted in November/2020 and the difficulty in obtaining laboratory animals due to the COVID-19 Pandemic, which caused the closure of most research centers.
2. The second limitation is time constraints. A PhD students have to meet deadlines for submitting a thesis. Therefore, the time available for the toxicity estimation of MgO/ZnO CS NPs on other organs (such as the heart, brain, stomach, bone marrow, etc.) was insufficient. So we recommend the need for a future study (e.g., a longitudinal toxicity study) to determine the helpful medical applications
3. Lack of previous research studies on the topic. Citing and referencing prior research studies constitutes the basis of the literature review for the study. To the best of our knowledge and according to a literature survey, no report is available on the acute lethal effect and toxicity of biologic MgO/ZnO CS NPs.

Conclusions

The composition of MgO/ZnO CS NPs, as confirmed by XRD and EDS analyses, was pure, with no impurity elements present. The TEM images show that the generated materials have NPs nature and morphology, the NPs are agglomerated, and total separation is impossible. The animals in all the groups did not show severe clinical poisoning symptoms that lead to mortality. The outcomes indicate

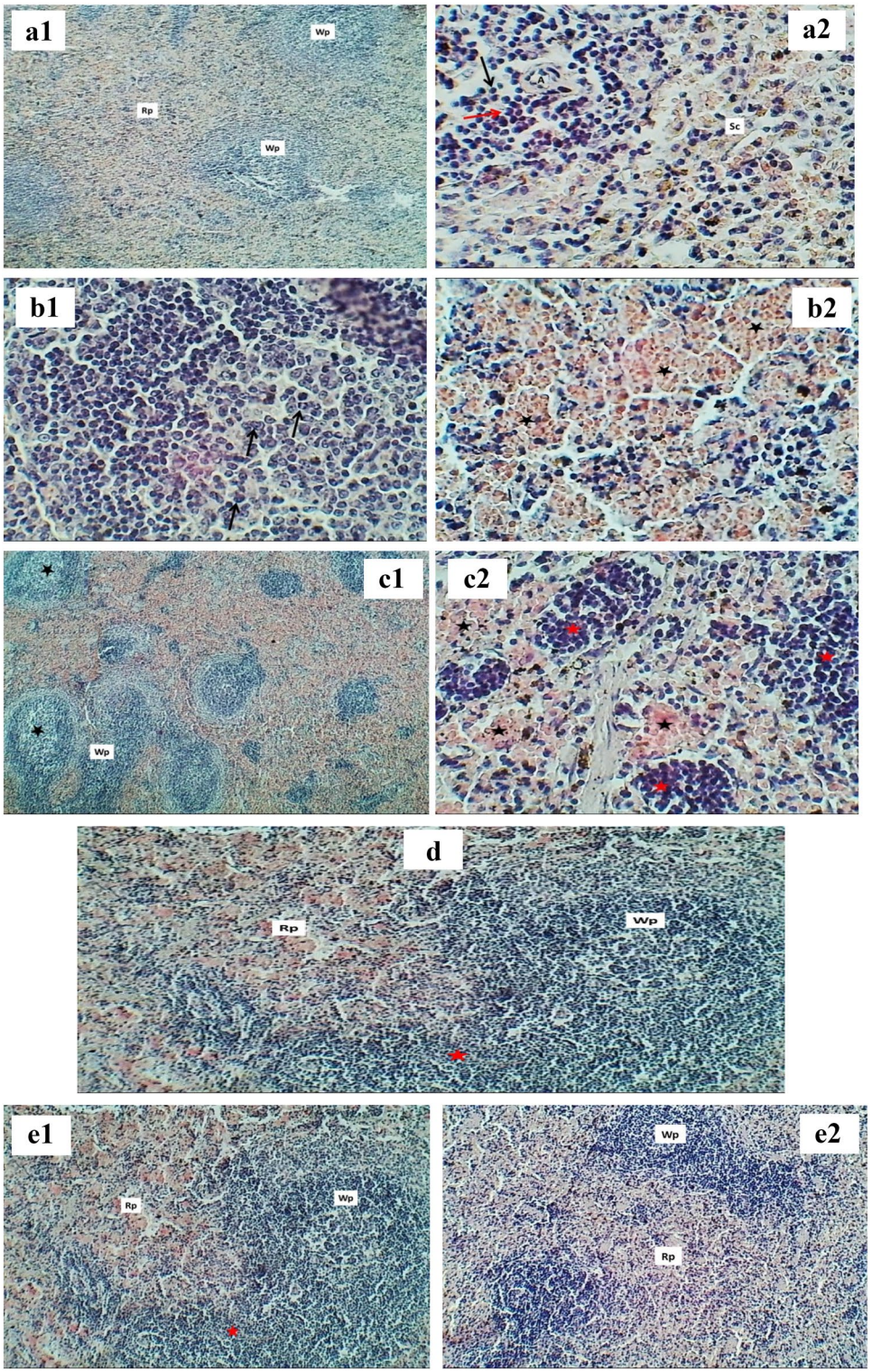

Fig. 8 Histological results of the spleen (H and E stained, ×400 magnification). **a** Section of the spleen in the control group. **a1** A section of the spleen shows a normal appearance of splenic white pulp (Wp) and Red pulp (Rp). **a2** Central arteriole (A) lymphocytes (black arrow), macrophage (red arrows) and splenic cord (Sc). **b** Histological results of the spleen after 30 days of oral exposure to MgO/ZnO CS NPs with 1.25 (mg L^{-1}) doses. **b1** Section of the splenic white shows marked lymphocytic hyperplasia (arrows). **b2** Section of spleen Red pulp shows marked dilation and congestion of splenic sinusoids (asterisks). **c** at 2.5 (mg L^{-1}) doses, **c1** section of the splenic white shows marked lymphocytic hyperplasia (asterisks) of white pulp (Wp). **c2** Section of spleen Red pulp shows marked dilation and congestion of splenic sinusoids (black asterisks) and focal groups of hyperplasia lymphocytes (Red asterisks). **d** At 5 (mg L^{-1}) doses. Section of the splenic white shows marked lymphocytic hyperplasia (asterisks) of white pulp (Wp). **e** At 10 (mg L^{-1}) doses. **e1** Spleen sections show a normal appearance of the splenic red pulp (Rp) and white pulp (Wp). **e2** Section of the spleen show the normal appearance of a lymphocytic follicle (red arrows) and splenic sinus (black arrow)

that the growth retardation of the female rats administered with MgO/ZnO CS NPs resulted from infection by hyperthyroidism. The insignificant effect of MgO/ZnO CS NPs on WBCs indicates that MgO/ZnO CS NPs have no harmful impact on the immune system. The significant increase in RBC, Hb, and HCT at the 10 mg L^{-1} dose indicates that these NPs stimulated the rate of blood corpuscle generation. NPs at these doses may be helpful in treating anemia. The increase in the T4 level indicates that the rats' infection was caused by hyperthyroidism. This finding may be useful in

regulating thyroid hormones and treating hypothyroid with a 1.2 mg L^{-1} dose of MgO/ZnO CS NPs due to its toxicity to the liver and the kidney. Our results suggest that the toxicity observed in the liver, kidney, and spleen of the female rats treated with MgO/ZnO CS NPs may be attributed to the enhanced ROS production by these NPs. Long-term exposure, during which rats adapt to the MgO/ZnO CS NPs exposure, maybe another factor of toxicity. This phenomenon prevents MgO/ZnO CS NPs from being fully absorbed or facilitates their excretion in large amounts, hence mitigating the toxicity in animals.

Acknowledgements The author would like to thank the support of the University of Al-Nahrain/Biotechnology Research Center/Animal House as well as the Plasma Physics laboratory at the Department of Physics, College of Science, University of Baghdad, Iraq.

Declarations

Conflict of Interests No conflict of interest among authors.

References

Ahamed M, Hisham Akhtar MJ, Alhadlaq HA, Alrokayan SA (2015) Assessment of the lung toxicity of copper oxide nanoparticles: current status. Nanomedicine 10(15):2365–2377. https://doi.org/10.2217/nnm.15.72

Ali AA, Rammah YS, El-Mallawany R, Souri D (2017) FTIR and UV spectra of pentaternary borate glasses. Measurement 105:72–77

Almansour MI, Mosaid AA, Shraideh ZA, Jarrar BM (2017) Zinc oxide nanoparticles hepatotoxicity: histological and histochemical study. Environ Toxicol Pharmacol 51:124–130. https://doi.org/10.1016/j.etap.2017.02.015

Aluko B, Oloyede OI, Molehin OR, Smith YRA (2017) Effect of acute doses of magnesium hydroxide nanoparticles on some biochemical parameters of wistar rats. Annu Res Rev Biol 21(6):1–11. https://doi.org/10.9734/ARRB/2017/38155

Ashafa AOT, Orekoya LO, Yakubu MT (2012) Toxicity profile of ethanolic extract of *Azadirachta indica* stem bark in male Wistar rats. Asian Pac Trop Biomed 2(10):811–817. https://doi.org/10.1016/S2221-1691(12)60234-2

Borysiewicz MA (2019) ZnO as a functional material, a review. Curr Comput-Aided Drug Des 9(10):505. https://doi.org/10.3390/cryst9100505

Bruggeman PJ, Kushner MJ, Locke BR, Gardeniers JGE, Graham WG, Graves DB et al (2016) Plasma–liquid interactions: a review and roadmap. Plasma Sources Sci Technol 25(5):053002. https://doi.org/10.1088/0963-0252/25/5/053002

Chen Q, Li J, Li Y (2015) A review of plasma–liquid interactions for nanomaterial synthesis. J Phys D Appl Phys 48(42):424005. https://doi.org/10.1088/0022-3727/48/42/424005

Chiang WH, Mariotti D, Sankaran RM, Eden JG, Ostrikov K (2019) Microplasmas for advanced materials and devices. Adv Mater 32(18):1905508. https://doi.org/10.1002/adma.201905508

Chinthala M, Balakrishnan A, Venkataraman P, Gowtham VM, Polagani RK (2021) Synthesis and applications of nano-MgO and composites for medicine, energy, and environmental remediation: a review. Environ Chem Lett 19(6):4415–4454. https://doi.org/10.1007/s10311-021-01299-4

Espinosa-Cristobal LF, Martinez-Castañon GA, Loyola-Rodriguez JP, Patiño-Marin N, Reyes-Macías JF, Vargas-Morales JM, Ruiz F (2013) Toxicity, distribution, and accumulation of silver nanoparticles in Wistar rats. J Nanopart Res 15(6):1702. https://doi.org/10.1007/s11051-013-1702-6

Hegemann D, Lorusso E, Butron-Garcia MI, Blanchard NE, Rupper P, Favia P, Heuberger M, Vandenbossche M (2016) Suppression of hydrophobic recovery by plasma polymer films with vertical chemical gradients. Langmuir 32(3):651–654. https://doi.org/10.1021/acs.langmuir.5b03913

Hornak J (2021) Synthesis, properties, and selected technical applications of magnesium oxide nanoparticles: a review. Int J Mol Sci 22(23):12752. https://doi.org/10.3390/ijms222312752

Jang HJ, Jung EY, Parsons T, Tae HS, Park ChS (2021) A Review of plasma synthesis methods for polymer films and nanoparticles under atmospheric pressure conditions. Polymers 13(14):2267. https://doi.org/10.3390/polym13142267

Jeyaraj M, Gurunathan S, Qasim M, Kang MH, Kim JH (2019) A Comprehensive review on the synthesis, characterization, and biomedical application of platinum nanoparticles. Nanomaterials 9(12):1719. https://doi.org/10.3390/nano9121719

Kaushik N, Linh NN, Ghimire B, Pengkit A, Sornsakdanuphap J, Lee SJ, Choi EH (2019) Plasma and nanomaterials: fabrication and biomedical applications. Nanomaterials 9(1):98. https://doi.org/10.3390/nano9010098

Khabbazi M, Harsij M, Hedayati SAA, Gholipoor H, Gerami MH, Farsani HG (2015) Effect of CuO nanoparticles on some hematological indices of rainbow trout *Oncorhynchus mykiss* and their potential toxicity. Nanomed J 2(1):67–73

Mangalampalliab B, Dumalaab N, Grover P (2017) Acute oral toxicity study of magnesium oxide nanoparticles and microparticles in female albino Wistar rats. Regul Toxicol Pharmacol 90:170–184. https://doi.org/10.1016/j.yrtph.2017.09.005

Mangalampalli B, Dumala N, Venkata RP, Grover P (2018) Genotoxicity, biochemical, and biodistribution studies of magnesium oxide nano and microparticles in albino wistar rats after 28-day repeated oral exposure. Environ Toxicol 33(4):396–410. https://doi.org/10.1002/tox.22526

Mirshafie V, Sun B, Chang ChH, Liao YP, Jiang W et al (2018) Toxicological profiling of metal oxide nanoparticles in liver context reveals pyroptosis in kupffer cells and macrophages versus apoptosis in hepatocytes. ACS Nano 12(4):3836–3852. https://doi.org/10.1021/acsnano.8b01086

Nguyen LN, Kaushik N, Lamichhane P, Mumtaz S, Paneru R et al (2020) In situ plasma-assisted synthesis of polydopamine-functionalized gold nanoparticles for biomedical applications. Green Chem 22(19):6588–6599. https://doi.org/10.1039/D0GC01348J

Peterson ME, Castellano CA, Rishniw M (2016) Evaluation of body weight, body condition, and muscle condition in cats with hyperthyroidism. J Vet Intern Med 30:1780–1789. https://doi.org/10.1111/jvim.14591

Rajabi SK, Sohrabnezhad Sh (2018) Fabrication and characteristic of Fe3O4@ MOR@ CuO core-shell for investigation antibacterial properties. J Fluor Chem 206:36–42. https://doi.org/10.1016/j.jfluchem.2017.12.010

Rao J, Bao L, Wang B, Fan M, Feo L (2018) Plasma surface modification and bonding enhancement for bamboo composites. Compos B Eng 138:157–167. https://doi.org/10.1016/j.compositesb.2017.11.025

Rumbach P, Bartels DM, Sankaran RM, Go DB (2015) The solvation of electrons by an atmospheric-pressure plasma. Nat Commun 6(1):7248. https://doi.org/10.1038/ncomms8248

Rumbach P, Go DB (2017) Perspectives on plasmas in contact with liquids for chemical processing and materials synthesis. Top Catal 60:799–811. https://doi.org/10.1007/s11244-017-0745-9

Rumbach P, Witzke M, Sankaran RM, Go DB (2013) Decoupling interfacial reactions between plasmas and liquids: charge transfer vs plasma neutral reactions. J Am Chem Soc 135(44):16264–16267. https://doi.org/10.1021/ja407149y

Sabale S, Kandesar P, Jadhav V, Komorek R, Motkuri RK, Yu XY (2017) Recent developments in the synthesis, properties, and biomedical applications of core/shell superparamagnetic iron oxide nanoparticles with gold. Biomater Sci 5(11):2212–2225. https://doi.org/10.1039/x0xx00000x

Sajid M, Ilyas M, Basheer Ch, Tariq M, Daud M et al (2014) Impact of nanoparticles on human and environment: review of toxicity factors, exposures, control strategies, and future prospects. Environ Sci Pollut Res 22(6):4122–4143. https://doi.org/10.1007/s11356-014-3994-1

Sakr S, Steenkamp V (2021) Zinc oxide nanoparticles induce oxidative stress and histopathological toxicity in the thyroid gland and liver of rats. Toxicol Environ Chem 103(4):399–422. https://doi.org/10.1080/02772248.2021.1941021

Seo HJ, Gil YE, Hwang KH, Ananth A, Boo JH (2019) Synthesis and characterization of plasma-polymer gate dielectric films for graphene field effect transistor devices. Electron Mater Lett 15(4):396–401. https://doi.org/10.1007/s13391-019-00139-6

Shakibaie M, Shahverdi AR, Faramarzi MA, Hassanzadeh GR, Rahimi HR, Sabzevari O (2013) Acute and subacute toxicity of novel biogenic selenium nanoparticles in mice. Pharm Biol 51(1):58–63. https://doi.org/10.3109/13880209.2012.710241

Singh N, Das MK, Gautam R, Ramteke A, Rajamani P (2019) Assessment of intermittent exposure of zinc oxide nanoparticle (ZNP)–mediated toxicity and biochemical alterations in the splenocytes of male Wistar rat. Environ Sci Pollut Res 26(32):33642–33653. https://doi.org/10.1007/s11356-019-06225-4

Vasani RB, Szili EJ, Rajeev G, Voelcker NH (2017) On-demand antimicrobial treatment with antibiotic-loaded porous silicon capped with a pH-responsive dual plasma polymer barrier. Chem Asian J 12(13):1605–1614. https://doi.org/10.1002/asia.201700427

Vasilev K (2013) Nanoengineered plasma polymer films for biomaterial applications. Plasma Chem Plasma Process 34(3):545–558. https://doi.org/10.1007/s11090-013-9506-0

Wojnarowicz J, Chudoba T, Lojkowski W (2020) A review of microwave synthesis of zinc oxide nanomaterials: reactants, process parameters and morphologies. Nanomaterials 10(6):1086. https://doi.org/10.3390/nano10061086

YaoY ZY, Qu J, Tang M, Zhang T (2019) The toxicity of metallic nanoparticles on liver: the subcellular damages, mechanisms, and outcomes. Int J Nanomed 14:8787–8804. https://doi.org/10.2147/IJN.S212907

Yousef MI, Al-Hamadani MYI, Kamel MA (2019) Reproductive toxicity of aluminum oxide nanoparticles and zinc oxide nanoparticles in male rats. Nanoparticle 1(1):3. https://doi.org/10.35702/nano.10002